Hydrogen dissociation on metal surfaces: A semi-empirical approach

Nour Ghassemi, E.

CHAPTER 3

Chemically Accurate Simulation of Dissociative Chemisorption of D_2 on Pt(111)

This chapter is based on:

Elham Nour Ghassemi, Mark Wijzenbroek, Mark F. Somers and Geert-Jan Kroes. Chemical Physics Letters **683**, 329-335, 2017.

Abstract

Using semi-empirical density functional theory and the quasi-classical trajectory (QCT) method, a specific reaction parameter (SRP) density functional is developed for the dissociation of dihydrogen on Pt(111). The validity of the QCT method was established by showing that QCT calculations on reaction of D_2 with Pt(111) closely reproduce quantum dynamics results for reaction of D_2 in its rovibrational ground state. With the SRP functional, QCT calculations reproduce experimental data on D_2 sticking to Pt(111) at normal and off-normal incidence with chemical accuracy. The dissociation of dihydrogen on Pt(111) is non-activated, exhibiting a minimum barrier height of -8 meV.

3.1 Introduction

The availability of accurate barriers for reactions of molecules on metal surfaces is of central importance to chemistry. Catalysis is used to make more than 80% of the chemicals produced worldwide [1], and the accurate calculation of the rate of a heterogeneously catalyzed process requires accurate barriers for the elementary surface reactions involved [2]. This is especially true for the rate controlling steps [3, 4], which often are dissociative chemisorption reactions.

Chemistry would thus benefit enormously from the availability of implementations of first principles methods that would enable the chemically accurate (*i.e.*, to within 1 kcal/mol) calculation of barriers for reactions of molecules with metal surfaces. However, presently such implementations do not yet exist [5]. Also, density functional theory (DFT) using functionals at the gradient approximation (GA) or meta-GA level, which can be used to map out potential energy surfaces (PESs) for molecules interacting with metals, is not yet capable of predicting reaction barriers for gas-phase reactions with chemical accuracy [6]. This accuracy problem of DFT is reflected in the limited accuracy with which absolute rates of heterogeneously catalyzed processes over model catalysts can now be computed with empirically optimized density functionals (*e.g.*, 2 orders of magnitude for ammonia production over Ru catalysts [7]).

Currently, the most viable route to chemically accurate barriers for molecules with metal surfaces uses implementations [8, 9] of specific reaction parameter DFT (SRP−DFT [10]). In this semi-empirical version of DFT, usually a single adjustable parameter in the density functional is fitted to reproduce an experiment that is particularly sensitive to the reaction barrier height for the specific system considered. Next, the quality of the functional is tested by checking that the candidate SRP density functional for the system also reproduces other experiments on the same system, which differ from the experiment the functional was fitted to in a non-trivial way [8, 9]. Using SRP−DFT we have recently started with an effort to develop a database of chemically accurate barriers for molecules reacting with metals, which can be used to benchmark implementations of first principles methods with a claim to chemical accuracy. This database now contains data for H_2 + Cu(111) [8], H_2 + Cu(100) [11], and CH_4 + Ni(111) [9].

The goal of this chapter is to extend the development of SRP density functionals, and the database, with a result for a weakly activated dissociative chemisorption reaction of H_2 with a transition metal surface. For this, we have selected the H_2 + Pt(111) system. Reasons for selecting this system are that Pt is an important hydrogenation catalyst [12], and that the interaction of H_2 with Pt(111) and other Pt surfaces has been investigated in a number of experimental [13–21] and theoretical [18, 22–29] studies.

Here, we fit an SRP density functional for H_2 + Pt(111) to dissociative chemisorption probabilities for D_2 + Pt(111) obtained from molecular beam measurements performed at normal incidence by Luntz *et al.* [15]. The quality of the functional is confirmed by showing that the functional also allows reaction probabilities to be reproduced with chemical accuracy for experiments performed at off-normal incidence [15]. This is a non-trivial result, as the reaction probability for D_2 + Pt(111) does not obey normal energy scaling [15], *i.e.*, it also depends on the component of the incidence energy parallel to the surface. This dependence arises from a particular type of correlation between the height of the barriers and their distance to the surface [23], the lowest barrier being furthest from the surface [25]. In view of the successes previously achieved for systems exhibiting a van der Waals well affecting the reactivity [9, 30], we adopt a SRP density functional in which the correlation functional [31] allows at least a qualitatively accurate description of the attractive part of the van der Waals interaction. The PBEα exchange functional [32] was adopted, which allows one not only to interpolate between the well-known RPBE [33] and PBE [34] functionals,

but also between PBE and a functional approximating the Wu-Cohen (WC) functional [35], which turned out to be important for the present case.

This chapter is set up as follows. In Section 3.2.1 we describe the dynamical model we used, and in Section 3.2.2 how the PES for H_2 + Pt(111) was obtained. Section 3.2.3 describes the dynamics methods employed, and Section 3.2.4 gives computational details. Section 3.3.1 describes the PES obtained with the SRP density functional. Section 3.3.2 considers the accuracy of the QCT method [36] with the PES employed, and the accuracy that might be achieved by performing dynamics calculations only for the rovibrational ground state of D_2, rather than performing a complete molecular beam simulation. In Section 3.3.3 we discuss how a candidate SRP density functional was derived for H_2 + Pt(111) through comparison to normal incidence data. In Section 3.3.4 we confirm the quality of the SRP functional through comparison of calculated sticking probabilities with experiments performed for off-normal incidence. Section 3.4 presents our conclusions and a brief outlook.

3.2 Method

3.2.1 Dynamical model

The calculations use the so-called Born-Oppenheimer static surface (BOSS) model [8]. As discussed in for instance Ref. [29], this model allows accurate calculations on reactive scattering of H_2 from metal surfaces. With the model, the calculation of reaction probabilities is split in two parts: First, the PES is calculated (Section 3.2.2), and next the PES is used in dynamics calculations (Section 3.2.3). In the PES and the dynamics calculations, only the six molecular degrees of freedom of the H_2 molecule are taken into account. The coordinates to describe the motion of the molecule are shown in Figure 3.1 (a).

3.2.2 Calculation of the PES

The ground state PES was calculated using DFT. The exchange-correlation (XC) functional used to compute the PES may be written as

$$E_{XC} = E_X^{PBE\alpha} + E_C^{vdW-DF2}, \tag{3.1}$$

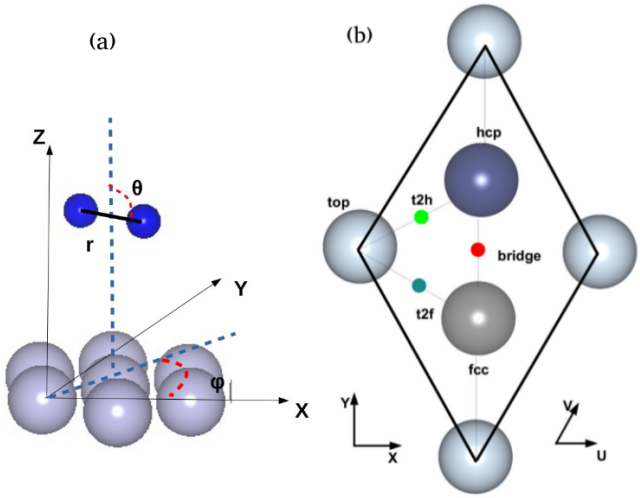

Figure 3.1: (a) The center of mass coordinate system used for the description of the H_2 molecule relative to the static Pt(111) surface. (b) The surface unit cell and the sites considered for the Pt(111) surface, and the relationship with the coordinate system chosen for H_2 relative to Pt(111). The origin $(X, Y, Z) = (0, 0, 0)$ of the center of mass coordinates is located in the surface plane at a top site. Polar and azimuthal angles θ and ϕ are chosen such that ($\theta = 90°$, $\phi = 0°$) corresponds to molecules parallel to the surface along the X (or equivalently U) direction.

i.e., we use the PBEα exchange functional [32], with α being the adjustable parameter, and the van der Waals DF2 functional of Langreth and Lundqvist and co-workers [31]. With the choice $\alpha = 1$ the PBEα functional corresponds [32] to the PBE functional [34], while for $\alpha \to \infty$ the PBEα functional corresponds [32] to the RPBE functional [33]. For $\alpha = 0.52$ a functional is obtained that closely resembles [32] the WC functional that performs well in solid state calculations [35]. The use of PBEα in semi-empirical applications would seem to be especially advantageous if interpolation is required between PBE and a less repulsive exchange functional; if the goal is to interpolate between PBE and RPBE exchange we suggest using a weighted average of these two [9, 37], as using $\alpha \to \infty$ in PBEα to

obtain the RPBE limit is a bit awkward for this purpose.

To obtain a global expression for the PES, the accurate corrugation reducing procedure (CRP) [38] was used to interpolate points calculated on a grid with DFT. The procedure used is exactly the same as used in Ref. [29]. The p3m1 plane group symmetry [39] associated with the Pt(111) surface was used.

3.2.3 Dynamics calculations of reaction probabilities

Reaction probabilities were calculated for the ($\nu = 0$, $j = 0$) state of D_2 with the time-dependent wave packet (TDWP) method [40] in an implementation for dihydrogen scattering from surfaces with hexagonal symmetry that is fully described in Ref. [25]. Dissociation probabilities of D_2 colliding with Pt(111) for comparison with molecular beam experiments on the same system [15] were calculated with the QCT method [36] in an implementation described in Ref. [29]. Earlier calculations predicted that even for the lighter H_2 molecule the QCT method yields dissociative chemisorption probabilities for hydrogen dissociation on Pt(111) that are in excellent agreement with quantum dynamics results [24]. For the best comparison with experiments, the calculations include Monte-Carlo averaging over the velocity distributions of the hydrogen beams, and Boltzmann averaging over the rovibrational states of hydrogen, as fully described in Ref. [29]. An important assumption made in our calculations is that the molecular beams used in the experiments of Luntz *et al.* [15] are quite similar to hydrogen beams produced in experiments of Juurlink and co-workers [41], and we used the beam parameters presented in table 3 of Ref. [30] to simulate D_2 beams in our work on the basis of this assumption.

3.2.4 Computational details

The DFT calculations were performed with the VASP (version 5.2.12) programme [42–44]. Standard projector augmented wave (PAW) potentials [45] were used. First, the bulk fcc lattice constant was determined in the same manner as used previously for H_2 + Au(111) [46], using a 20 × 20 × 20 Γ−centered grid of k-points. With the optimized SRP density functional (using $\alpha = 0.57$, see Section 3.3) a lattice constant of 4.015 Å was obtained, in reasonable agreement with the experimental value of 3.91 Å. Next, a relaxed 5-layer slab was obtained, again in the same manner as

used before for H_2 + Au(111) [46], using a 20 × 20 × 1 Γ−centered grid of k-points. After having obtained the relaxed slab, single point calculations were carried out on H_2 + Pt(111), using a 9 × 9 × 1 Γ−centered grid of k-points, and a plane wave cut-off of 400 eV, in a super cell approach in which 13 Å of vacuum length was used for the spacing between the Pt(111) slabs and a (2 × 2) surface unit cell. The grid of the points for which the H_2 + Pt(111) calculations were done, and other details of the calculations, were taken the same as in Ref. [29]. The CRP PES was extrapolated to the gas-phase potential of H_2 in the same way as used in Ref. [29].

In the QCT calculation of dissociative chemisorption probabilities for comparison with molecular beam experiments, 10000 trajectories were run for each (ν, j) state with the vibrational quantum number $\nu \leq 3$ and the rotational quantum number $j \leq 20$. For each j, uniform sampling was performed of the magnetic rotational quantum number m_j. The centre-of-mass of H_2 was originally placed at $Z = 9$ Å, with the velocity directed towards the surface and sampled from appropriate velocity distributions for D_2 beams (see table 3 of Ref. [30]). The molecule is considered dissociated once $r > 2.25$ Å, and considered scattered once $Z > 9$ Å. Other computational details of the QCT calculations are the same as in Ref. [29]. The surface lattice constant (*i.e.*, the nearest neighbor Pt−Pt distance) used in the QCT calculations (and in the TDWP calculations) was taken as the computed Pt lattice constant divided by $\sqrt{2}$ (*i.e.*, as 2.84 Å).

In the TDWP calculations on ($\nu = 0$, $j = 0$) D_2 + Pt(111), two separate wave packet calculations were performed to cover the collision energy range $E_i = 0.05 - 0.55$ eV. This procedure avoids problems that may arise from the interaction of the low energy components of the wave packet with optical potentials if only one broad wave packet is used to cover a very large translational energy range. The input parameters we used in the TDWP calculations are listed in table 3.1. Convergence tests carried out suggest that, with the use of these parameters, the reaction probabilities computed for ($\nu = 0$, $j = 0$) D_2 are converged to within better than 2 % of their values (*i.e.*, relative errors ≤ 2 %).

Table 3.1: Input parameter for the quantum dynamical calculations of D_2 dissociating on Pt(111). All values are given in atomic units. The abbreviation "sp" refers to the specular grid used to bring in the initial wave function.

Parameter	**Description**	**Value**	**Value**
E_i	normal incidence range in Z	[0.05-0.20]eV	[0.15-0.55]eV
$N_X = N_Y$	no. of grid points in X and Y	16	16
N_Z	no. of grid points in Z	256	128
$N_{Z(sp)}$	no. of specular grid points	256	256
ΔZ	spacing of Z grid points	0.135	0.135
Z_{min}	minimum value of Z	-1.0	-1.0
N_r	no. of grid points in r	40	48
Δr	spacing of r grid points	0.2	0.17
r_{min}	minimum value of r	0.4	0.4
j_{max}	maximum j value in basis set	24	24
m_{jmax}	maximum m_j value in basis set	16	16
Δt	time step	5	5
T_{tot}	propagation time	82000	22000
Z_0	center of initial wave packet	16.955	16.955
$Z_{\inf}$	location of analysis line	12.5	12.5
Z^{opt}_{start}	start of optical potential in Z	12.5	12.5
Z^{opt}_{end}	end of optical potential in Z	33.425	16.145
A_Z	optical potential strength in Z	0.00072	0.0045
r^{opt}_{start}	start of optical potential in r	4.2	4.2
r^{opt}_{end}	end of optical potential in r	8.2	8.4
A_r	optical potential strength in r	0.0096	0.0096
$Z(sp)^{opt}_{start}$	start of optical potential in $Z(sp)$	22.355	22.355
$Z(sp)^{opt}_{end}$	end of optical potential in $Z(sp)$	33.425	33.425
$A_{Z(sp)}$	optical potential strength in $Z(sp)$	0.0035	0.0035

Table 3.2: Barrier heights (E_b), the distance to the surface of the barrier (Z_b), and the H−H distance at the barrier (r_b, in Å) are given for four different dissociation geometries defined by the impact site and the angle ϕ (see Figure 3.1), for dissociation of H_2 over Pt(111) with H_2 parallel to the surface ($\theta = 90°$). The results have been obtained with the PBEα-vdW-DF2 functional with $\alpha = 0.57$. For the top site, results are given for two barrier geometries. The E_b values in brackets correspond to the 6D PES computed with the Becke-Perdew functional (see Ref. [25]).

site	ϕ **(degrees)**	$\mathbf{E_b}$ **(eV)**	$\mathbf{r_b}$ **(Å)**	$\mathbf{Z_b}$ **(Å)**
top, early	0	-0.008 (0.06)	0.769	2.202
top, late	0	-0.055	1.096	1.549
bridge	0	0.275 (0.27)	0.837	1.777
hcp	30	0.462 (0.42)	0.874	1.586
t2h	120	0.200 (0.20)	0.837	1.679

3.3 Results and discussion

3.3.1 Potential energy surface

Two-dimensional cuts (so-called elbow plots) through the PES used in the dynamics calculations on H_2 + Pt(111) are shown in Figure 3.2, in all cases for H_2 oriented parallel to the surface. With the optimized SRP density functional (using $\alpha = 0.57$, see Section 3.3.3), the dissociation is non-activated in the sense that the transition state has an energy that is 8 meV below the gas-phase minimum energy of H_2 (the early barrier for dissociation above the top site, see also table 3.2, which lists the geometries and barrier heights corresponding to the results shown in Figure 3.2). With the functional used, the barrier height (E_b) shows a larger energetic corrugation (*i.e.*, a greater variation with impact site) than previously obtained with the Becke-Perdew functional (Ref. [25] and references therein). This is what should be expected for a functional accurately describing the experiments on dissociative chemisorption of D_2 on Pt(111) [15] , as the previously computed sticking probability vs. incident translational energy curve was too steep [18, 24]. Note that previous experience with H_2-metal systems suggests that the use of Lundqvist-Langreth van der Waals cor-

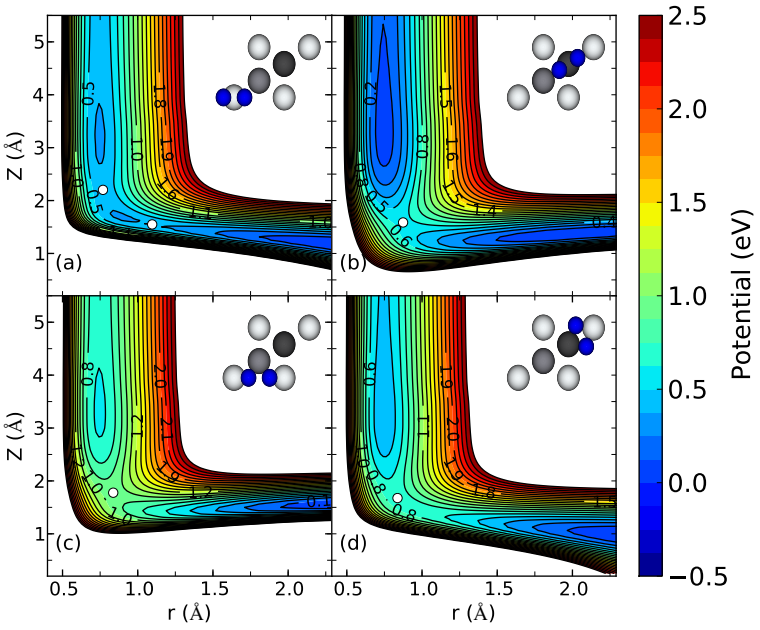

Figure 3.2: Elbow plots (*i.e.* $V(Z, r)$) resulting from the H_2 + Pt(111) PES computed with the PBEα-vdW-DF2 functional with $\alpha = 0.57$, and interpolated with the CRP method for four high symmetry configurations with the molecular axis parallel to the surface ($\theta = 90°$), for (a) the top site and $\phi = 0°$, (b) the hcp site and $\phi = 30°$, (c) the bridge site and $\phi = 0°$ (bridge-to-top), and (d) the t2h site and $\phi = 120°$ (see also Figure 3.1). Barrier geometries are indicated with white circles, and the corresponding barrier heights are given in table 3.2.

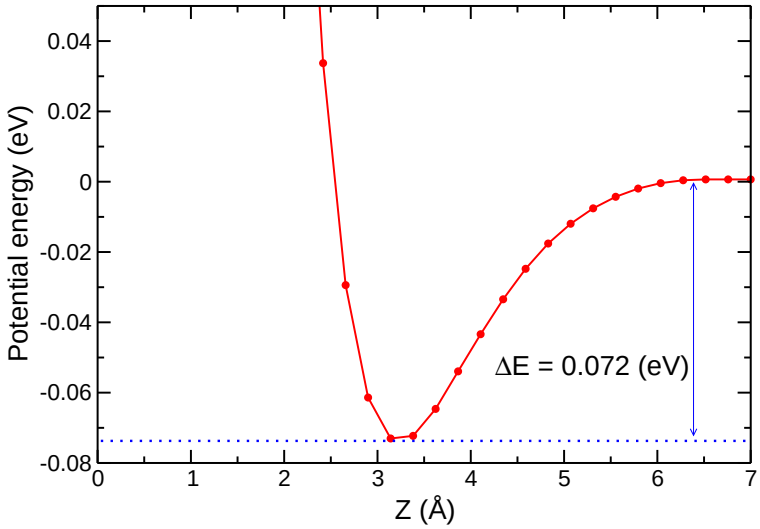

Figure 3.3: The potential for H_2 + Pt(111) is shown as a function of the molecule-surface distance, for $r = r_e$ after averaging over the four remaining molecular degrees of freedom. The results are for the PES computed with the PBEα-vdW-DF2 functional with $\alpha = 0.57$.

relation functionals, as employed here, yield PESs with larger energetic corrugation than ordinary generalized gradient approximation (GGA) correlation functionals [29, 30].

Figure 3.3 shows a plot of the potential at $r = r_e$, after averaging over X, Y, θ, and ϕ, with r_e being the minimum H−H distance of gas-phase H_2. This averaged potential curve shows a van der Waals minimum well depth of 72 meV, in excellent agreement with the range of values found in experiments (*i.e.*, 55 meV [14, 18], and 76 meV [47]). Getting the van der Waals attractive interaction right may be important to obtaining a correct value for the energy of the "early" transition state (which occurs at $Z = 2.2$ Å, see table 3.2) and is probably also important to the calculation of probabilities for diffractive scattering, for which detailed experimental results are available [18] (see also Chapter 6).

3.3.2 Quantum vs. quasi-classical dynamics, and the importance of simulating the molecular beam

Figure 3.4 (a) shows a comparison of reaction probabilities computed for D_2 in its initial ($\nu = 0,\ j = 0$) state for specific incidence energies with quantum dynamics and with quasi-classical dynamics. The calculations used the optimized SRP density functional (*i.e.*, with $\alpha = 0.57$, see Section 3.3.3). Even in the absence of averaging over initial rovibrational states and over the distribution of energies, as would be appropriate for comparisons with molecular beam experiments, the quantum and QCT results are in excellent agreement with one another. In the following, we will therefore use the QCT method to compute sticking probabilities for comparison to the molecular beam experiments of Luntz *et al.* [15].

Figure 3.4 (b) shows a comparison of reaction probabilities computed with the QCT method for D_2 in its initial ($\nu = 0,\ j = 0$) state for specific incidence energies with QCT results obtained with full averaging over the rovibrational state populations and velocity distributions that are typical for molecular beam experiments using pure D_2 beams [30, 41]. The comparison of Figure 3.4 (b) suggests that it should not really be necessary to take the effect of the velocity distribution and the rovibrational state distribution into account, in broad agreement with an earlier theoretical study of H_2 + Pt(111) [27]. This is in sharp contrast with findings for the highly activated H_2 + Cu(111) reaction [8, 48]; for this system, taking into account the velocity distribution is necessary for accurate results, because the reactivity may come entirely from incidence energies above the average incidence energy of the beam, and above the high reaction threshold. Even though taking into account the beam conditions should be much less important for D_2 + Pt(111), in the following we will always represent computational results with full averaging over the incidence energy and rovibrational state population of the D_2 beams, to obtain the best possible comparison with the molecular beam experiments of Luntz *et al.* [15].

3.3.3 Fit of the SRP density functional to molecular beam data for normal incidence

Before the SRP functional for H_2 + Pt(111) could be fit, a choice had to be made concerning which experimental dataset for normal incidence theoretical results should be compared with. In the literature at the time

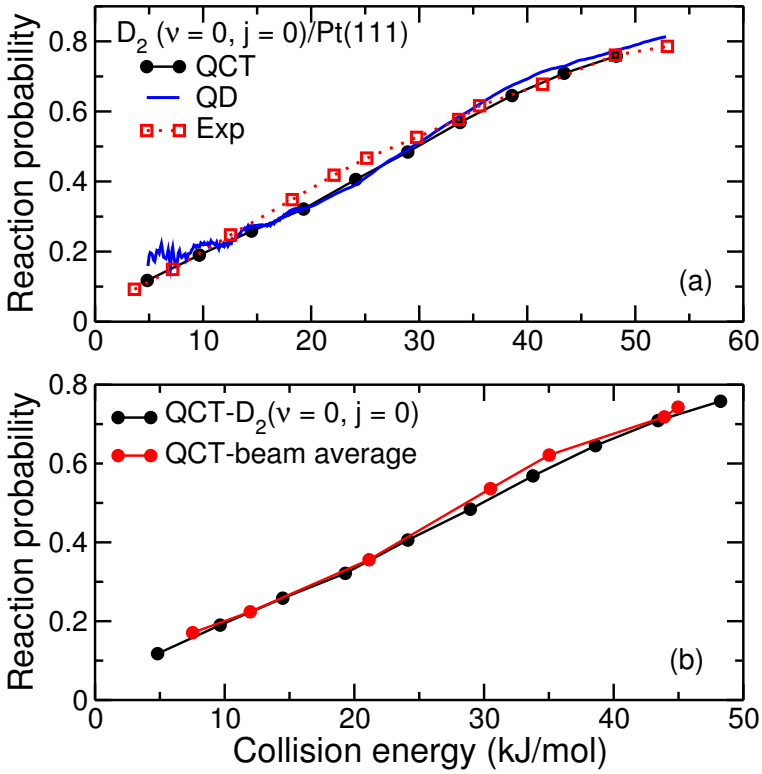

Figure 3.4: (a) Dissociation probabilities computed for ($\nu = 0, j = 0$) D_2 + Pt(111) with quantum dynamics and with the QCT method are shown as a function of the collision energy, for normal incidence. The results are compared with sticking probabilities measured for D_2 + Pt(111) [15] and shown as a function of average incidence energy. (b) Dissociation probabilities computed for ($\nu = 0,\ j = 0$) D_2 + Pt(111) with the QCT method for specific collision energies are compared with sticking probabilities computed for D_2 + Pt(111) with full averaging over the rovibrational state populations and velocity distributions of typical molecular beams of pure D_2.

our research was performed, two sets of molecular beam data were available for dihydrogen normally incident on Pt(111), *i.e.*, those of Luntz *et al.* [15] and those of Samson *et al.* [16]. The work of Luntz *et al.* focused on the dihydrogen + Pt(111) system, looking at the effects of the angle of incidence θ_i, surface temperature T_s, isotopic mass, and nozzle temperature T_n in great detail, and producing data for D_2 + Pt(111) at T_s = 300 K for a large range of incidence energies E_i by also using seeding of D_2 in H_2 to achieve high E_i. In contrast, Samson *et al.* only published data for D_2 + Pt(111) for normal incidence, for one value of T_s (150 K), for the more limited range of E_i available with pure D_2 beams only, in a paper focused on how alloying varying amounts of Sn into the surface affects the sticking. Furthermore, Luntz *et al.* explicitly stated that their "incidence energies" (labeled E_i in their work) were energy averaged over the TOF[1] distribution of the beams they used, whereas Samson *et al.* simply assumed that the average incidence energy (which we will label as $\langle E_i \rangle$) is given by $\langle E_i \rangle = 2.75\ k_B T_n$. For these reasons, we have chosen to fit our SRP functional to the normal incidence data of Luntz *et al.*, assuming that these would represent the most accurate dataset.

The assumption that the dataset of Luntz *et al.* is best for benchmarking purposes is important. Although Samson *et al.* stated that their D_2 + Pt(111) data closely reproduce the prior results of Luntz *et al.*, plotting the datasets together reveals that the data of Samson *et al.* are displaced along the energy axis by 1 to 1.5 kcal/mol relative to the Luntz *et al.* data, towards higher energies (not shown in this chapter). The data of Samson *et al.* therefore suggest a somewhat less reactive surface. If our assumption is incorrect, or if our interpretation of the meaning of $\langle E_i \rangle$ in the experiments of Luntz *et al.* would be incorrect (we obtain the average by averaging incidence energy over the flux weighted velocity distribution given by equation 3 in the Supporting Information to Ref. [8]) this should be reflected in the accuracy of the extracted SRP functional and minimum barrier height. Problems with the interpretation of results of molecular beam experiments due to lacking or incomplete specification of the velocity distributions have hampered efforts to obtain accurate SRP functionals and benchmark data before [49]. However, the problem noted here for H_2 + Pt(111) is not as severe as for H_2 + Pd(111) [49]. See also Chapter 6 for a detailed discussion of the experiments of the two different groups, and the

[1] time-of-flight

quality of the SRP functional in describing these experiments.

To obtain an SRP functional, first tests were performed combining the PBE functional for exchange [34] with the Lundqvist-Langreth functional of Dion *et al.* (vdW-DF1) [50]. With this functional, the van der Waals well was too deep compared with experimental results, and the computed reaction probabilities were shifted to too high energies and did not exhibit chemical accuracy (results not shown). For these reasons, we switched to the improved Lundqvist-Langreth functional of Lee *et al.* (vdW-DF2) [31], and to the PBEα functional [32], adjusting α by trial and error to obtain agreement with the sticking experiments of Luntz *et al.* [15]. By choosing $\alpha = 0.57$, agreement with the experiments for normal incidence could be obtained to within chemical accuracy, by which we mean that the computed sticking probabilities are displaced along the energy axis from the interpolated experimental curve by no more than 1 kcal/mol (see Figure 3.5). The resulting SRP−DFT PES shows a minimum barrier height of -8 meV ($\approx$ 1 kJ/mol), suggesting the reaction to be non-activated if the molecule hits the surface at the right site (the top site, see table 3.2). The "activated appearance" of the reaction probability curve comes from the molecule also hitting the surface at other impact sites and orientations for which higher barriers are encountered (see for instance table 3.2 and Figure 3.2), as already suggested by Luntz *et al.* at the time of their work [15].

3.3.4 Confirming the quality of the SRP density functional by comparison to molecular beam data for off-normal incidence

Strictly speaking, the functional obtained in Section 3.3.4 is, at this stage, only a "candidate SRP functional": to become an SRP functional, dynamics calculations with the functional should also be able to reproduce other experiments on the same system, which differ from the experiments the functional was fit to in a non-trivial way [8, 9]. For this, we chose to use the datasets obtained by Luntz *et al.* for off-normal incidence [15]. For H_2 + Pt(111) more recent, detailed data on molecular diffraction are also available [18], but recent work on H_2 + Ru(0001) suggests that accurately reproducing diffraction data is fraught with difficulties [30] (see also Chapter 6). This is most likely related to the need to extrapolate the experimental data to a low temperature or even static surface regime using Debye-Waller attenuation, or to simulate the effect of surface temperature

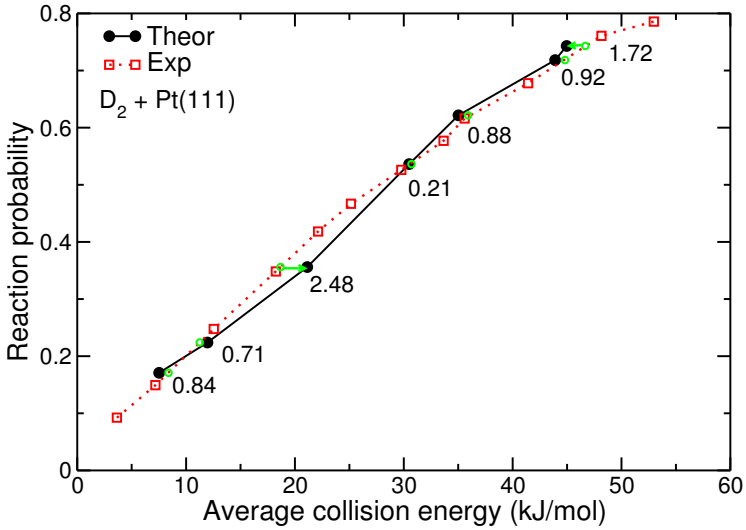

Figure 3.5: Reaction probabilities computed for D_2 + Pt(111) with the SRP density functional (see text) are shown as a function of $\langle E_i \rangle$, comparing to the molecular beam results of Luntz *et al.* [15]. The results are for normal incidence. The arrows and accompanying numbers show the collision energy spacing (in kJ/mol, 1 kcal/mol $\approx$ 4.2 kJ/mol) between the computed sticking probabilities and the interpolated experimental sticking probability data (green circles).

in accurate quantum dynamics calculations [30].

Reaction probabilities computed for $\theta_i = 30°$ and $45°$ agree with the experimental values to within chemical accuracy (Figure 3.6). Larger displacements than 1 kcal/mol of the computed reaction probabilities from the interpolated experimental sticking curve are observed for $\theta_i = 60°$, but we argue that for this large an incidence angle our operational definition of chemical accuracy may not be appropriate. The slope of the measured sticking curve as a function of total incidence energy is small, so that a small error in the measured reaction probability could have a large effect on the energy displacement of the computed reaction probability to the interpolated experimental curve. In this context, we note that error bars on the measured sticking probabilities were lacking [15]. In view of the positive results for $\theta_i = 30°$ and $45°$, we argue that our PBEα-vdW-DF2 functional

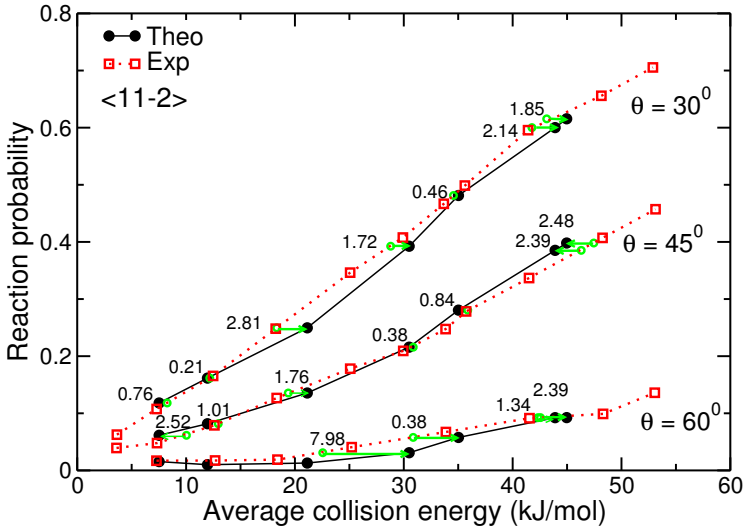

Figure 3.6: Reaction probabilities computed for D_2 + Pt(111) with the SRP density functional (see text) are shown as a function of , comparing to the molecular beam results of Luntz *et al.* [15]. The results are for off-normal incidence at the indicated incidence angles θ_i of 30°, 45° and 60°, along the ⟨11-2⟩ incidence direction. The arrows and accompanying numbers show the collision energy spacing (in kJ/mol, 1 kcal/mol ≈ 4.2 kJ/mol) between the computed sticking probabilities and the interpolated experimental sticking probability data (green circles).

is an SRP functional for H_2 + Pt(111), and that the minimum barrier data (and the barriers obtained for other impact sites shown in table 3.2) can be used for benchmark purposes, *i.e.*, they can be included in an emerging database with chemically accurate barriers for molecules interacting with transition metals [5].

Luntz *et al.* did not specify the incidence plane used in their experiments on off-normal incidence [15]. The computed data shown in Figure 3.6 are for incidence along the $\langle 11-2\rangle$ direction, which corresponds to the vector bisecting the U and V vectors in Figure 3.1. However, for incidence along the $\langle 10-1\rangle$ direction (corresponding to the direction of U in Figure 3.1), the computed sticking probabilities closely reproduce the values computed for the $\langle 11-2\rangle$ direction, and they likewise reproduce the experimental

data, for $\theta_i = 30°$ and $45°$ (not shown). For $\theta_i = 60°$ and incidence along the $\langle 10-1 \rangle$ direction, the computed sticking probabilities do not quite reproduce the values computed for the $\langle 11-2 \rangle$ direction (in agreement with earlier theoretical work on H_2 + Pt(111) [25]), but the result that for this incidence direction and large angle the computed data do not reproduce the experiments with chemical accuracy is also obtained for the $\langle 10-1 \rangle$ direction.

3.4 Conclusions and outlook

We have obtained an SRP density functional for H_2 + Pt(111) by adjusting the α parameter in the PBEα-vdW-DF2 functional until reaction probabilities computed with the QCT method reproduced sticking probabilities measured for normally incident D_2 with chemical accuracy. In the QCT calculations, the rovibrational state populations and the velocity distributions of the incident beams were taken into account. Also, the appropriateness of the use of the QCT method for the purpose of accurately calculating reaction probabilities for D_2 + Pt(111) was established by a comparison with quantum dynamics calculations for the initial ($\nu = 0,\ j = 0$) state of D_2. The quality of the SRP functional was confirmed by showing that QCT calculations using the functional also reproduced data for off-normal incidence for $\theta_i = 30°$ and $45°$, for which the computed reaction probabilities show no dependence on the plane of incidence. The minimum barrier height obtained for the reaction is -8 meV, in agreement with the experimental observation of no, or only a small energetic threshold to reaction [15]. This value can be entered into a small [5], but growing [9] database with barriers of reactions of molecules with metal surfaces, for which chemical accuracy is claimed.

Our conclusion depends on the assumption that the data of Luntz *et al.* are accurate and the validity of our interpretation of the average incidence energy in their experiments [15] (see Section 3.3.3). To confirm this, accurate new experiments on reaction of H_2 or D_2 with Pt(111) for varying incidence angles and well-defined molecular beam velocity distributions and incidence plane would be welcomed. Experiments that were done [51] after the research presented in this chapter only suggested small differences between reaction probabilities measured for the $\langle 10-1 \rangle$ and $\langle 11-1 \rangle$ incidence directions and $\theta_i = 50°$.

Future computational work could address the question of how the dynamical model may have to be extended to accurately reproduce the detailed molecular diffraction data available for H_2 + Pt(111) [18] (see also Chapter 6). Once such a model is available it could be used in further tests of the SRP density functional for H_2 + Pt(111) by comparison to these data, and in tests of the candidate SRP density functional for H_2 + Ru(0001), for which detailed diffraction data are also available [30]. We also suggest that the SRP functional be used to model data on the reaction of H_2 with stepped Pt surfaces [20, 21], to check whether SRP functionals developed for a low index transition metal surface exhibit transferability to systems in which the same molecule interacts with a vicinal or stepped surface of that metal. This question will be considered for Pt(211) in Chapter 5.

References

1. Noyori, R. Synthesizing Our Future. *Nature Chemistry,* 5–6 (2009).
2. Xu, Y. *et al.* In Silico Search for Novel Methane Steam Reforming Catalysts. *New Journal of Physics* **15,** 125021 (2013).
3. Wolcott, C. A., Medford, A. J., Studt, F. & Campbell, C. T. Degree of Rate Control Approach to Computational Catalyst Screening. *Journal of Catalysis* **330,** 197–207 (2015).
4. Sabbe, M. K., Reyniers, M.-F. & Reuter, K. First-Principles Kinetic Modeling in Heterogeneous Catalysis: An Industrial Perspective on Best-Practice, Gaps and Needs. *Catalysis Science & Technology* **2,** 2010–2024 (2012).
5. Kroes, G. J. Toward a Database of Chemically Accurate Barrier Heights for Reactions of Molecules with Metal Surfaces. *Journal of Physical Chemistry Letters* **6,** 4106–4114 (2015).
6. Peverati, R. & Truhlar, D. G. Quest for a Universal Density Functional: the Accuracy of Density Functionals Across a Broad Spectrum of Databases in Chemistry and Physics. *Philosophical Transactions of the Royal Society A: Mathematical, Physical and Engineering Sciences* **372,** 20120476 (2014).
7. Medford, A. J. *et al.* Assessing the Reliability of Calculated Catalytic Ammonia Synthesis Rates. *Science* **345,** 197–200 (2014).
8. Díaz, C. *et al.* Chemically Accurate Simulation of a Prototypical Surface Reaction: H_2 Dissociation on Cu(111). *Science* **326,** 832–834 (2009).
9. Nattino, F. *et al.* Chemically Accurate Simulation of a Polyatomic Molecule-Metal Surface Reaction. *Journal of Physical Chemistry Letters* **7,** 2402–2406 (2016).
10. Chuang, Y.-Y., Radhakrishnan, M. L., Fast, P. L., Cramer, C. J. & Truhlar, D. G. Direct Dynamics for Free Radical Kinetics in Solution: Solvent Effect on the Rate Constant for the Reaction of Methanol with Atomic Hydrogen. *Journal of Physical Chemistry A* **103,** 4893–4909 (1999).

11. Sementa, L. *et al.* Reactive Scattering of H_2 from Cu(100): Comparison of Dynamics Calculations Based on the Specific Reaction Parameter Approach to Density Functional Theory with Experiment. *Journal of Chemical Physics* **138** (2013).

12. D. Navalikhina, M. & V. Krylov, O. Heterogeneous Catalysts of Hydrogenation. *Russian Chemical Review* **67,** 587–616 (1998).

13. Cowin, J. P., Yu, C., Sibener, S. J. & Hurst, J. E. Bound Level Resonances in Rotationally Inelastic HD/Pt (111) Surface Scattering. *Journal of Chemical Physics* **75,** 1033–1034 (1981).

14. Cowin, J. P., Yu, C., Sibener, S. J. & Wharton, L. HD Scattering from Pt(111): Rotational Excitation Probabilities. *Journal of Chemical Physics* **79,** 3537–3549 (1983).

15. Luntz, A. C., Brown, J. K. & Williams, M. D. Molecular Beam Studies of H_2 and D_2 Dissociative Chemisorption on Pt(111). *Journal of Chemical Physics* **93,** 5240–5246 (1990).

16. Samson, P., Nesbitt, A., Koel, B. E. & Hodgson, A. Deuterium Dissociation on Ordered Sn/Pt(111) Surface Alloys. *Journal of Chemical Physics* **109,** 3255–3264 (1998).

17. Gee, A. T., Hayden, B. E., Mormiche, C. & Nunney, T. S. The Role of Steps in the Dynamics of Hydrogen Dissociation on Pt(533). *Journal of Chemical Physics* **112,** 7660–7668 (2000).

18. Nieto, P. *et al.* Reactive and Nonreactive Scattering of H_2 from a Metal Surface Is Electronically Adiabatic. *Science* **312,** 86–89 (2006).

19. Poelsema, B., Lenz, K. & Comsa, G. The Dissociative Adsorption of Hydrogen on Pt(111): Actuation and Acceleration by Atomic Defects. *Journal of Chemical Physics* **134** (2011).

20. Groot, I. M. N., Kleyn, A. W. & Juurlink, L. B. F. The Energy Dependence of the Ratio of Step and Terrace Reactivity for H_2 Dissociation on Stepped Platinum. *Angewandte Chemie International Edition* **50,** 5174–5177 (2011).

21. Groot, I. M. N., Kleyn, A. W. & Juurlink, L. B. F. Separating Catalytic Activity at Edges and Terraces on Platinum: Hydrogen Dissociation. *Journal of Physical Chemistry C* **117,** 9266–9274 (2013).

22. Halstead, D. & Holloway, S. Quantum-Mechanical Scattering of H_2 from Metal Surfaces: Diffraction and Dissociative Adsorption. *Journal of Chemical Physics* **88,** 7197–7208 (1988).

23. Darling, G. R. & Holloway, S. The Role of Parallel Momentum in the Dissociative Adsorption of H_2 at Highly Corrugated Surfaces. *Surface Science* **304,** L461–L467 (1994).

24. Pijper, E. *et al.* Six-Dimensional Quantum Dynamics of Scattering of (v=0, j=0) H_2 from Pt(1 1 1): Comparison to Experiment and to Classical Dynamics Results. *Chemical Physics Letters* **347,** 277–284 (2001).

25. Pijper, E., Kroes, G. J., Olsen, R. A. & Baerends, E. J. Reactive and Diffractive Scattering of H_2 from Pt(111) Studied Using a Six-Dimensional Wave Packet Method. *Journal of Chemical Physics* **117,** 5885–5898 (2002).

26. Pijper, E., Kroes, G. J., Olsen, R. A. & Baerends, E. J. Dissociative and Diffractive Scattering of H_2 from Pt(111): A Four-Dimensional Quantum Dynamics Study. *Journal of Chemical Physics* **116,** 9435–9448 (2002).

27. Vincent, J., Olsen, R., Kroes, G. J. & Baerends, E. Dissociative Chemisorption of H_2 on Pt(1 1 1): Isotope Effect and Effects of the Rotational Distribution and Energy Dispersion. *Surface Science* **573,** 433–445 (2004).

28. Ludwig, J. & Vlachos, D. G. *Ab Initio* Molecular Dynamics of Hydrogen Dissociation on Metal Surfaces Using Neural Networks and Novelty Sampling. *Journal of Chemical Physics* **127** (2007).

29. Wijzenbroek, M., Klein, D. M., Smits, B., Somers, M. F. & Kroes, G. J. Performance of a Non-Local van der Waals Density Functional on the Dissociation of H_2 on Metal Surfaces. *Journal of Physical Chemistry A* **119,** 12146–12158 (2015).

30. Wijzenbroek, M. & Kroes, G. J. The Effect of the Exchange-Correlation Functional on H_2 Dissociation on Ru(0001). *Journal of Chemical Physics* **140** (2014).

31. Lee, K., Murray, É. D., Kong, L., Lundqvist, B. I. & Langreth, D. C. Higher-Accuracy van der Waals Density Functional. *Physical Review B* **82,** 081101 (2010).

32. Madsen, G. K. H. Functional Form of the Generalized Gradient Approximation for Exchange: The PBEα Functional. *Physical Review B* **75,** 195108 (2007).

33. Hammer, B., Hansen, L. B. & Nørskov, J. K. Improved Adsorption Energetics within Density-Functional Theory Using Revised Perdew-Burke-Ernzerhof Functionals. *Physical Review B* **59,** 7413–7421 (1999).

34. Perdew, J. P., Burke, K. & Ernzerhof, M. Generalized Gradient Approximation Made Simple. *Physical Review Letters* **77,** 3865–3868 (1996).

35. Wu, Z. & Cohen, R. E. More Accurate Generalized Gradient Approximation for Solids. *Physical Review B* **73,** 235116 (2006).

36. Karplus, M., Porter, R. N. & Sharma, R. D. Exchange Reactions with Activation Energy. I. Simple Barrier Potential for (H, H_2). *Journal of Chemical Physics* **43,** 3259–3287 (1965).

37. Nattino, F., Díaz, C., Jackson, B. & Kroes, G. J. Effect of Surface Motion on the Rotational Quadrupole Alignment Parameter of D_2 Reacting on Cu(111). *Physical Review Letters* **108,** 236104 (2012).

38. Busnengo, H. F., Salin, A. & Dong, W. Representation of the 6D Potential Energy Surface for a Diatomic Molecule Near a Solid Surface. *Journal of Chemical Physics* **112,** 7641–7651 (2000).

39. Frankcombe, T. J., Collins, M. A. & Zhang, D. H. Modified Shepard Interpolation of Gas-Surface Potential Energy Surfaces with Strict Plane Group Symmetry and Translational Periodicity. *Journal of Chemical Physics* **137** (2012).

40. Kosloff, R. Time-Dependent Quantum-Mechanical Methods for Molecular Dynamics. *Journal of Physical Chemistry* **92,** 2087–2100 (1988).

41. Groot, I. M. N., Ueta, H., van der Niet, M. J. T. C., Kleyn, A. W. & Juurlink, L. B. F. Supersonic Molecular Beam Studies of Dissociative Adsorption of H_2 on Ru(0001). *Journal of Chemical Physics* **127,** 244701 (2007).

42. Kresse, G. & Furthmüller, J. Efficient Iterative Schemes for *Ab Initio* Total-Energy Calculations Using a Plane-Wave Basis Set. *Physical Review B* **54,** 11169–11186 (1996).

43. Kresse, G. & Furthmüller, J. Efficiency of *Ab-Initio* Total Energy Calculations for Metals and Semiconductors Using a Plane-Wave Basis Set. *Computational Materials Science* **6,** 15–50 (1996).

44. Kresse, G. & Hafner, J. *Ab Initio* Molecular Dynamics for Liquid Metals. *Physical Review B* **47,** 558–561 (1993).

45. Kresse, G. & Joubert, D. From Ultrasoft Pseudopotentials to the Projector Augmented-Wave Method. *Physical Review B* **59,** 1758–1775 (1999).

46. Wijzenbroek, M., Helstone, D., Meyer, J. & Kroes, G. J. Dynamics of H_2 Dissociation on the Close-Packed (111) Surface of the Noblest Metal: H_2 + Au(111). *Journal of Chemical Physics* **145,** 144701 (2016).

47. Poelsema, B., Lenz, K. & Comsa, G. The Dissociative Adsorption of Hydrogen on Defect-'Free' Pt(111). *Journal of Physics: Condensed Matter* **22,** 304006 (2010).

48. Kroes, G. J. & Díaz, C. Quantum and Classical Dynamics of Reactive Scattering of H_2 from Metal Surfaces. *Chemical Society Reviews* **45,** 3658–3700 (2016).

49. Boereboom, J. M., Wijzenbroek, M., Somers, M. F. & Kroes, G. J. Towards a Specific Reaction Parameter Density Functional for Reactive Scattering of H_2 from Pd(111). *Journal of Chemical Physics* **139** (2013).

50. Dion, M., Rydberg, H., Schröder, E., Langreth, D. C. & Lundqvist, B. I. van der Waals Density Functional for General Geometries. *Physical Review Letters* **92,** 246401 (2004).

51. Cao, K., van Lent, R., Kleyn, A. & Juurlink, L. A Molecular Beam Study of D_2 Dissociation on Pt(111): Testing SRP-DFT Calculations. *Chemical Physics Letters* **706,** 680–683 (2018).